Check for updates

Local aortic aneurysm wall expansion measured with automated image analysis

Jordan B. Stoecker, MD,[a] Kevin C. Eddinger, MD,[a] Alison M. Pouch, PhD,[b,c] Amey Vrudhula, BS,[d] *and* Benjamin M. Jackson, MD,[a] *Philadelphia, Pa; and New York, NY*

ABSTRACT

Background: Assessment of regional aortic wall deformation (RAWD) might better predict for abdominal aortic aneurysm (AAA) rupture than the maximal aortic diameter or growth rate. Using sequential computed tomography angiograms (CTAs), we developed a streamlined, semiautomated method of computing RAWD using deformable image registration (dirRAWD).

Methods: Paired sequential CTAs performed 1 to 2 years apart of 15 patients with AAAs of various shapes and sizes were selected. Using each patient's initial CTA, the luminal and aortic wall surfaces were segmented both manually and semiautomatically. Next, the same patient's follow-up CTA was aligned with the first using automated rigid image registration. Deformable image registration was then used to calculate the local aneurysm wall expansion between the sequential scans (dirRAWD). To measure technique accuracy, the deformable registration results were compared with the local displacement of anatomic landmarks (fiducial markers), such as the origin of the inferior mesenteric artery and/or aortic wall calcifications. Additionally, for each patient, the maximal RAWD was manually measured for each aneurysm and was compared with the dirRAWD at the same location.

Results: The technique was successful in all patients. The mean landmark displacement error was 0.59 ± 0.93 mm with no difference between true landmark displacement and deformable registration landmark displacement by Wilcoxon rank sum test ($P = .39$). The absolute difference between the manually measured maximal RAWD and dirRAWD was 0.27 ± 0.23 mm, with a relative difference of 7.9% and no difference using the Wilcoxon rank sum test ($P = .69$). No differences were found in the maximal dirRAWD when derived using a purely manual AAA segmentation compared with using semiautomated AAA segmentation ($P = .55$).

Conclusions: We found accurate and automated RAWD measurements were feasible with clinically insignificant errors. Using semiautomated AAA segmentations for deformable image registration methods did not alter maximal dirRAWD accuracy compared with using manual AAA segmentations. Future work will compare dirRAWD with finite element analysis–derived regional wall stress and determine whether dirRAWD might serve as an independent predictor of rupture risk. (JVS–Vascular Science 2022;3:48-63.)

Clinical Relevance: Current abdominal aortic aneurysm (AAA) surveillance methods are limited to assessments of the maximal diameter, which cannot accurately predict for AAA expansion and rupture risk. Automated assessment of AAA expansion across the entire three-dimensional geometry of the aneurysm could better describe aneurysm growth and could substantially inform management decisions, including the indications for repair. We have developed an accurate and streamlined approach to assessing local three-dimensional AAA expansion with submillimeter accuracy using computed tomography imaging obtained during routine aneurysm surveillance. This novel process does not require significant user expertise nor computer processing power and can be performed using open-source software readily accessible to both scientists and clinicians.

Keywords: Aneurysms; Biomechanics; Computational analysis and simulation

From the Division of Vascular Surgery and Endovascular Therapy, Department of Surgery,[a] and Division of Radiology,[b] Hospital of the University of Pennsylvania, Philadelphia; the Department of Bioengineering, University of Pennsylvania, Philadelphia[c]; and the Icahn School of Medicine at Mount Sinai, New York.[d]

Author conflict of interest: none.

Presented as a poster abstract at the 2020 Biomedical Engineering Society Annual Meeting, October 14-17, 2020 ONLINE and the 2020 Society for Vascular Surgery Vascular Research Initiatives Conference, November 5-12, 2020 ONLINE.

Correspondence: Jordan B. Stoecker, MD, Division of Vascular Surgery and Endovascular Therapy, Department of Surgery, Hospital of the University of Pennsylvania, 3400 Spruce St, 4th FL, Silverstein Bldg, Philadelphia, PA 19146 (e-mail: jordan.stoecker@pennmedicine.upenn.edu).

The editors and reviewers of this article have no relevant financial relationships to disclose per the JVS-Vascular Science policy that requires reviewers to decline review of any manuscript for which they may have a conflict of interest.

2666-3503

Copyright © 2021 by the Society for Vascular Surgery. Published by Elsevier Inc. This is an open access article under the CC BY-NC-ND license (http://creativecommons.org/licenses/by-nc-nd/4.0/).

https://doi.org/10.1016/j.jvssci.2021.11.004

The detected prevalence of asymptomatic abdominal aortic aneurysms (AAAs) has increased as noninvasive screening modalities have become more widely available. Aortic diseases, including aortic aneurysms, are the 12th leading cause of death in the United States.[1] AAA rupture is a major source of morbidity and mortality, with reported mortality rates of 40% to 50%.[2] Surgical intervention for asymptomatic patients has generally been reserved for those with an aortic diameter >5.5 cm or with an aneurysm expansion rate >10 mm/y. However, a previous autopsy study estimated that 10% to 24% of ruptured AAAs will be <5.5 cm in diameter.[3] Another study reported that 7% had had a diameter of <5.0 cm.[4] Thus, improved risk stratification of AAAs could prevent rupture and save lives.

Maximum diameter measurements on computed tomography (CT) angiograms (CTAs) have been previously shown to have an error in the range of 2 to 5 mm, which can limit its clinical utility.[5,6] This has been especially notable for noncircular aneurysms and when the centerline of the aorta is not axially oriented, which will hamper the accuracy of the measured aneurysm diameter in the axial plane.[5,6] Given that the management recommendations have been based on the thresholds of the size and growth rate, a diameter-based measurement technique can lead to treatment recommendations that are either overly aggressive or conservative owing to measurement error. To better assess aneurysm growth from surveillance imaging scans, prior literature has examined the role of the aortic cross-sectional area or volumetric changes. Although these appear more sensitive to detecting overall aneurysm growth, they cannot confer any information regarding localized aortic changes.[7,8]

It has been previously demonstrated that complex geometric properties of AAAs, including the curvature, shape, and degree of mural thrombus, can be superior to the maximal diameter measurements alone in predicting for aneurysm growth and possible rupture. Furthermore, changes in aneurysm tortuosity over time have been suggested as a potential marker during aneurysm surveillance.[9] However, many of these properties have remained cumbersome to calculate, are nonstandardized, and difficult to interpret for those without significant bioengineering knowledge. Therefore, these have not translated into clinical practice and appear unlikely to become relevant in the near future.[10-14] Therefore, although research into novel methods of aneurysm surveillance has been significant, maximal diameter measurements and growth in the maximal diameter have remained the default, yet suboptimal, clinical parameters.

Regional aortic wall deformation (RAWD) can be calculated using deformable image registration (dirRAWD).[13,15] This technique allows for quantification of aneurysm disease progression on surveillance imaging, with the ability to calculate the degree of shape changes between two rigidly registered CT images, a process previously called vascular deformation mapping. The benefits of assessing dirRAWD include the simple interpretation, high accuracy, and the ability to determine both radial and longitudinal aortic changes. Furthermore, because aortic rupture customarily occurs in a focal area of the aortic surface, RAWD might better assess for the risk of the clinically significant event one would like to predict. Although deformable image registration is rapidly being applied to neurologic and pulmonary disease processes, it has infrequently been applied to the field of vascular surgery, with no effects yet in clinical practice.[14,16-19]

A continued need exists for a more sensitive and accurate method of measuring the changes in aortic aneurysm dimensions, considering that the accurate detection of small magnitude changes has important implications for improving the understanding of aortic aneurysm progression and better informing treatment decisions. The aim of the present study was to develop a novel, semiautomated deformable image registration pipeline that can be applied to routine clinical surveillance CTA studies of patients with AAAs. We compared the results of the RAWD analysis with routine clinical CTA assessments to better understand the potential benefits and limitations of this technique. Our hypothesis was that the proposed deformation analysis technique could be accurately implemented and require minimal user input and that the results would favorably compare with the results obtained from both manual deformation and AAA diameter growth assessments.

ARTICLE HIGHLIGHTS

- **Type of Research:** A prospective, experimental research study
- **Key Findings:** We developed a streamlined, semiautomated method of computing local aneurysm expansion using deformable image registration in patients with computed tomography scans performed 1 to 2 years apart. Our algorithm demonstrated high accuracy in a cohort of 15 patients, with a submillimeter measurement error of 0.27 ± 0.23 mm and a relative error of 7.9%.
- **Take Home Message:** Our work has demonstrated that calculating local aneurysm expansion is feasible using open-source software and minimal user training and could serve as an independent predictor of rupture risk in the future.

METHODS

Population. Sequential surveillance CTAs of 15 patients with infrarenal AAAs of various shapes, sizes, and the extent of luminal thrombus from 2014 to 2018 were selected by querying the University of Pennsylvania

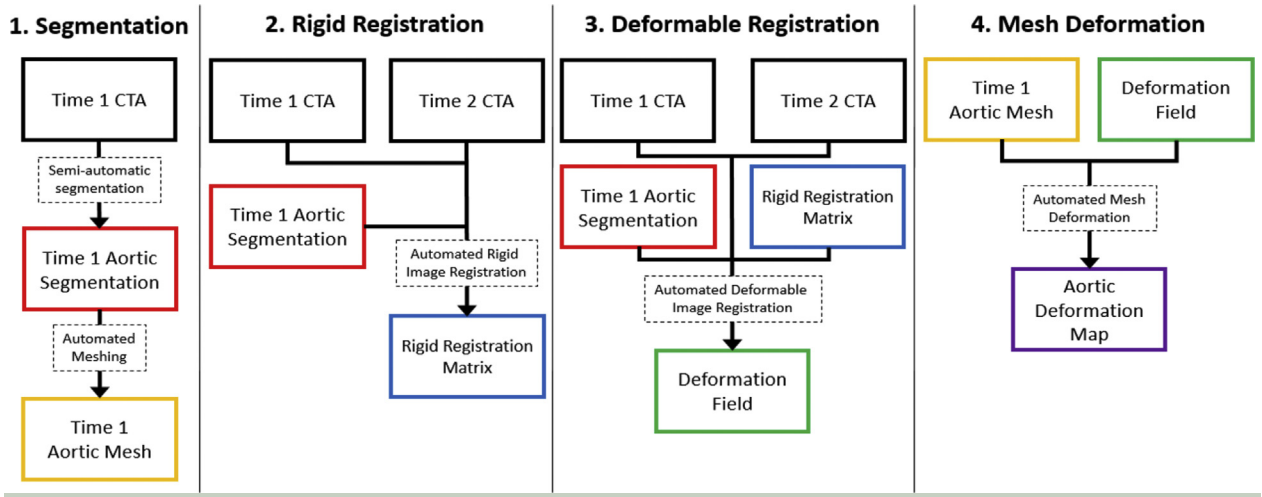

Fig 1. Overview of algorithm used to calculate regional aortic wall deformation (RAWD) with deformable image registration (dirRAWD) between sequential computed tomography angiograms (*CTAs*) and generation of aortic deformation map.

Health System PACS (picture archiving and communication system) database using Nuance mPower (Nuance Communications Inc, Burlington, Mass). The initial CTA scans were evaluated using radiology workstations and Sectra IDS7 (Sectra AB, Linköping, Sweden) and TeraRecon (TeraRecon Inc, Foster City, Calif). The inclusion criteria were age >18 years at the initial imaging study, the presence of infrarenal fusiform AAAs without evidence of rupture, and at least two sequential CTA studies performed within the health care system separated by 12 to 24 months. The patients were excluded if the aneurysm in question had ruptured or if the patient had undergone endovascular or open repair of the aneurysm in the interval between the imaging studies. The institutional review board expedited the review and approved the present study owing to the use of previously collected and anonymized data.

RAWD algorithm. The complete image processing and analysis pipeline, constituting the current approach to measuring dirRAWD, has been diagrammed in Fig 1. Raw data from the patients' CTA scans were anonymized and exported into DICOM (digital imaging and communications in medicine) format. ITK-SNAP (available at: http://www.itksnap.org/pmwiki/pmwiki.php; Penn Image Computing and Science Laboratory, Philadelphia, Pa) was used for segmentation and rigid registration of each patient's baseline CTA scan[20] (Supplementary Fig). In brief, ITK-SNAP is an open-source platform for medical image analysis that includes functionalities for manual image tracing and semiautomated segmentation using three-dimensional (3D) active contours and machine learning and a registration feature for the rigid alignment of images. In the present study, the images did not require application of filters or augmentation of Hounsfield units. Multilabel segmentations of the aortic lumen, aortic wall, and thrombus were created for all baseline CTAs (Fig 2). The aortic segmentation was performed by one physician, both manually and using a semiautomated process (using either active contour evolution based on Hounsfield unit thresholding or tissue classification), with the two methods compared for accuracy using the Dice coefficient. The semiautomated segmentation was inspected and manually corrected if required. The Dice coefficient is commonly used to assess for agreement between segmentation images. The Dice coefficient ranges from 0 (no overlap) to 1 (perfect overlap) and is defined as follows:

$$Dice = \frac{2 * Number\ of\ Overlapping\ Voxels}{Total\ Number\ of\ Voxels\ in\ Both\ Images\ Combined}$$

After segmentation of the baseline scan, the baseline and follow-up CTA images were aligned using automated rigid multiresolution image registration and the mutual information similarity metric in ITK-SNAP. The initial rigid registration was performed using a multiresolution scheme with 16× to 8× down-sampling to grossly align the images. Rigid registration was then repeated with computation of the similarity metric confined to the dilated aortic segmentation, first with 4× down-sampling and then at full resolution. Manual inspection was performed on all rigidly registered images to confirm adequate alignment (Fig 2).

After rigid image registration, deformable registration was performed using *greedy* (available at: https://sites.google.com/view/greedyreg/home; Penn Image Computing and Science Laboratory) to automatically generate a deformation field between the baseline and follow-up CTA images.[21] This open-source application has shown efficiency and accuracy for both CT and

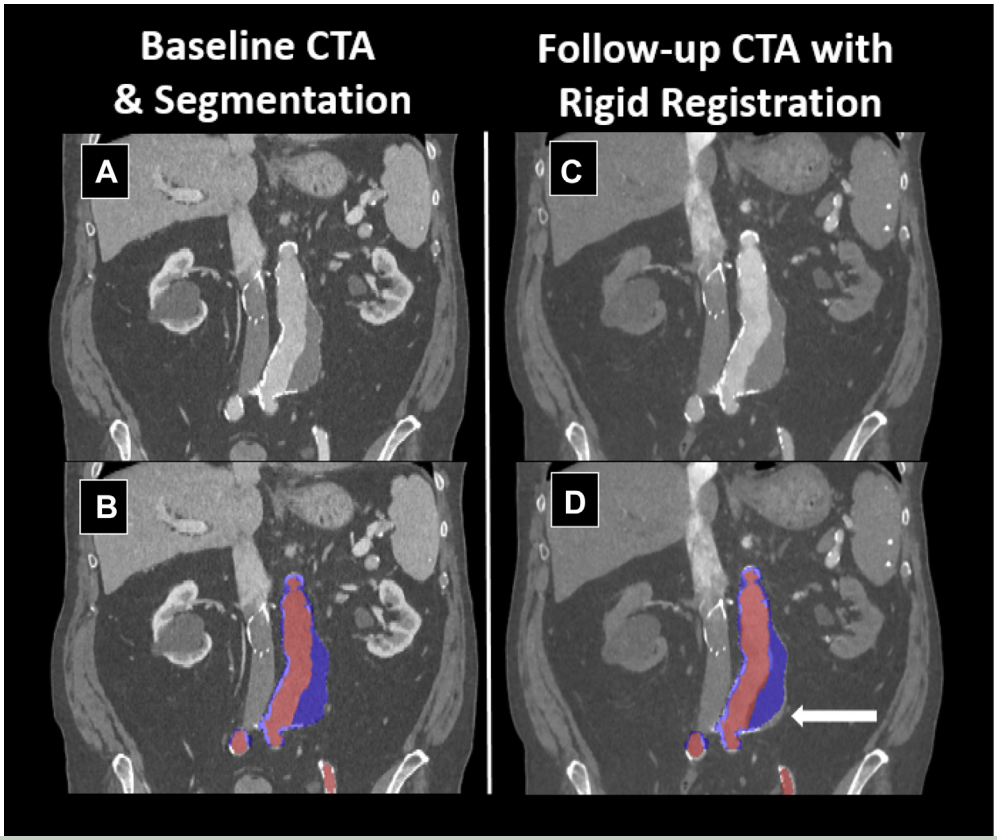

Fig 2. Baseline computed tomography angiogram (CTA; **A**) and overlay of multilabel aortic aneurysm segmentation **(B)**. On the right, the rigidly registered follow-up CTA is displayed **(C)** with overlay of the baseline segmentation **(D)**. The *white arrow* denotes the local aortic expansion that occurred between performance of the two CTAs.

magnetic resonance imaging. For deformable image registration, we used a normalized cross-correlation similarity metric with gradient descent optimization for 100 iterations at a course level (4×), 50 iterations at an intermediate level (2×), and 20 iterations at full resolution. For further algorithm optimization, the deformable registration was limited to a 10 × 10 × 10 neighborhood around each voxel, and the baseline aortic segmentation was dilated by 1.5 cm and used to restrict the deformation algorithm to the area of interest. A smoothing gradient with a sigma of 1.732 voxel was applied to the image match metric at each voxel, and the entire deformation field was smoothed with a gradient sigma of 0.707 voxel after each iteration to limit error and generate a smooth field. The deformable image registration equations and smoothing gradients used have been previously described in great detail.[22,23]

A mesh of the outer wall of the aorta was then automatically generated from the segmentation of the baseline CTA image using ITK-SNAP. The deformation field obtained by registration of the baseline image and follow-up scan was applied to this baseline outer aortic wall mesh, producing an aortic deformation map with local dirRAWD at every vertex on the mesh. This mesh can be displayed as a "heatmap" of the outer aortic wall, with the magnitude of deformation displayed at every mesh vertex to describe the local change in that region of the aorta over the period between the baseline and follow-up CTA scans. An example of the final results from the image analysis pipeline are shown in Fig 3.

To assess the accuracy of this algorithm in determining dirRAWD, the maximal RAWD was manually determined (manRAWD) for each patient. This was performed using the manual aortic segmentation and rigidly registered images, with manual measurement of the magnitude of displacement in the aortic outer wall between the baseline and follow-up images and the region of most expansion. This measured maximal manRAWD was considered the "true maximal deformation" and was compared to the algorithm-derived dirRAWD in the corresponding aortic wall region for assessment of accuracy. To assess segmentation intraobserver variability, all manual and semiautomated segmentations were performed twice by the same individual. Comparisons were then performed between the calculated dirRAWD using the repeat segmentation compared with the original to determine the relative intraobserver variability introduced by the segmentation process.

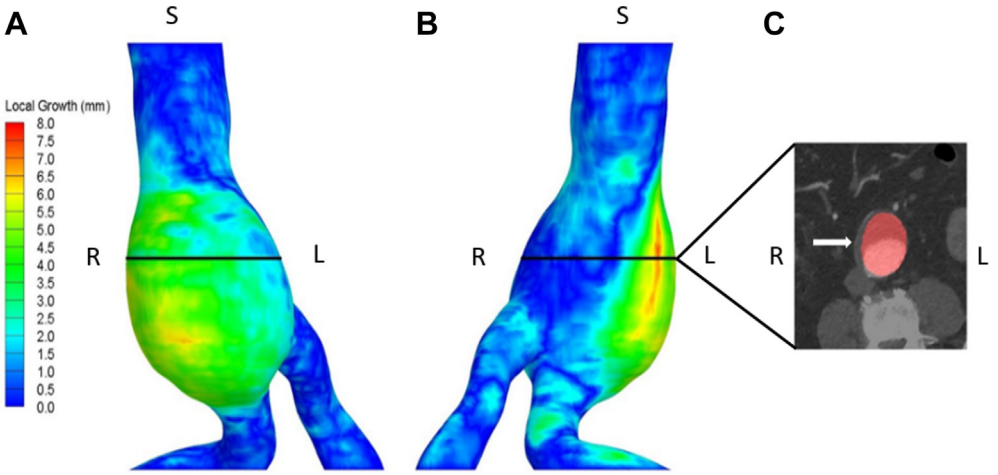

Fig 3. Local aortic deformation map shown from anterior **(A)** and posterior **(B)** perspectives. **C,** Slice of second computed tomography angiogram (CTA) from the indicated level, with an overlay of the initial aorta size in *red* and a *white arrow* denoting the degree of local expansion between the sequential CTAs.

Furthermore, to assess our algorithm's accuracy, the landmark displacement error was calculated using a fiduciary marker. First, the following landmark regions were defined in the baseline CTA: the inferior mesenteric artery and aortic wall calcifications >4 mm in size. Next, the deformation field generated from the dirRAWD algorithm was applied to displace the landmarks from the baseline CTA. The deformed landmark locations on the baseline CTA were compared against their true locations on the follow-up CTA to determine the displacement error in our algorithm.

The maximal aortic diameter was determined for all baseline and follow-up scans using axial measurements of the aneurysm and confirmed by measurements of the aortic segmentation (in mm). The aortic expansion rate was defined as the difference in the maximal aortic diameter between the baseline and follow-up CTAs during the study period between images (mm/y). These manually determined measurements were compared with the results from the radiology reports with no differences noted. The image analysis and calculations were performed on a system with 8 GB of RAM (random access memory) and Intel Core i5-8350 central processing unit.

Statistical analysis and image generation. Statistical analysis was performed using STATA (StataCorp, College Station, Tex). Plots were generated using Tecplot (Tecplot, Inc, Bellevue, Wash) and MeshLab (MeshLab, University of Pisa, Pisa, Italy). Nonparametric statistical analysis was used because of the small study population. Continuous variables were assessed using the Wilcoxon signed rank test when comparing two paired groups or Friedman's analysis of variance test when comparing three paired groups. Categorical variables were compared using the Fischer exact test. The relationships between the initial maximal aortic diameter, aortic expansion rate, and maximal deformation were calculated using the Pearson correlation coefficient. All P values were two-sided, and $P < .05$ was considered to indicate statistical significance. Logistic and linear regression modeling were used for binary and continuous outcomes, respectively. All results are presented as the mean ± standard deviation, unless otherwise specified. To eliminate the outliers, maximal deformation was defined as the 97.5th percentile of each aorta. A Dice score >0.7 has been previously suggested as an appropriate benchmark for image validation and was used in the present study.[24]

RESULTS

The technique was successful for all 15 patients, with initial demographic data shown in Table I and the Supplementary Table. The results for four example cases are shown in Fig 4. The average patient age was 66.7 ± 11.3 years, and the average interval between the sequential scans was 16.1 ± 2.7 months. The average baseline aortic diameter was 42.7 ± 9.9 mm, the average follow-up aortic diameter was 48.3 ± 11.8 mm, the mean aortic expansion rate was 4.5 ± 2.6 mm/y, and the mean true maximal deformation rate was 4.3 ± 2.5 mm/y. Seven patients (47%) had had aortic expansion rates of >5 mm/y (an indication of rapid growth). The manual aortic segmentation and semiautomated aortic segmentation for each aortic aneurysm showed agreement with a Dice score of 0.92 ± 0.02. On visual inspection, seven of the semiautomated aortic segmentations (47%) required no manual correction, six (40%) had required <2 minutes of correction, two (13%) had required <5 minutes of correction, and one aneurysm with extensive intraluminal thrombus had required 10 minutes of manual correction. The total time for rigid image registration was <2 minutes for all patients, and the total time for deformable image registration was <15 minutes in 14 of the 15 patients.

Table I. Demographics of 15 included patients

Demographic	Value
Age, years	66.7 ± 11.3 (46-83)
Male sex	9 (60)
History of hypertension	10 (67)
History of statin use	7 (47)
Family history of vascular aneurysms	3 (20)
Follow-up duration, months	16.1 ± 2.7 (13-22)
Initial aortic diameter, mm	42.7 ± 9.9 (31-60)
Final aortic diameter, mm	48.3 ± 11.8 (34-66)
Radiographic expansion rate, mm/y	4.5 ± 2.6 (0.5-9.3)
True maximal deformation (manRAWD), mm/y	4.3 ± 2.5 (1.2-9.2)

manRAWD, Maximal regional aortic wall deformation was manually determined.
Data presented as mean ± standard deviation (range) or number (%).

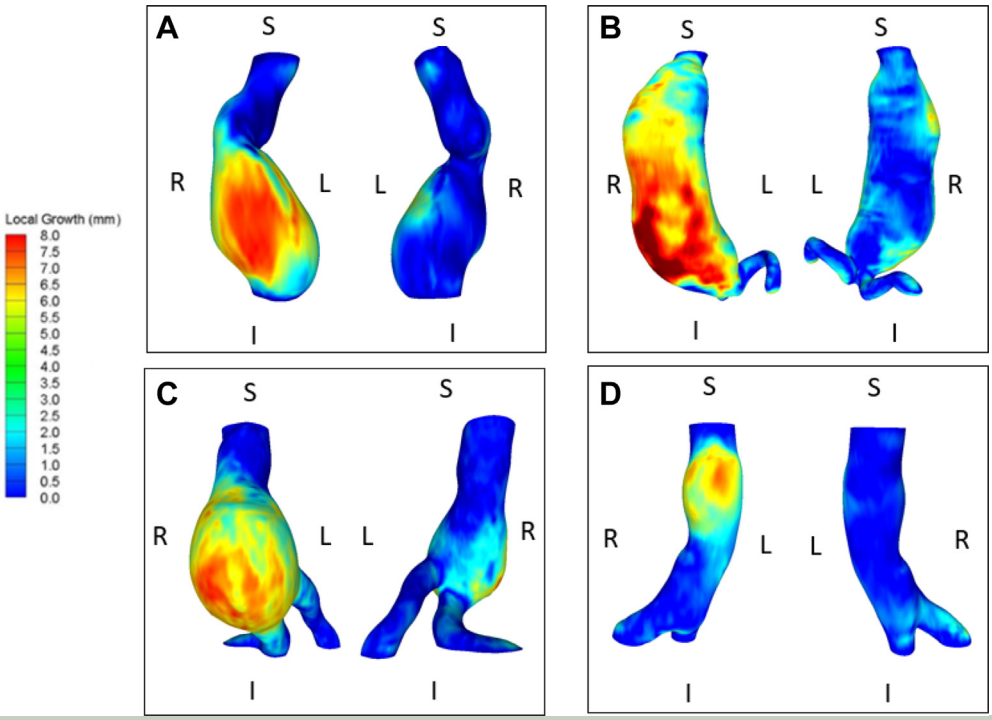

Fig 4. A-D, Four example results of regional aortic wall deformation (RAWD) with deformable image registration (dirRAWD) aortic maps generated by our algorithm.

Maximal deformation accuracy assessment. The maximal manRAWD, dirRAWD at the same location derived using the manual AAA segmentation, and dirRAWD at the same location derived using the semiautomated AAA segmentation are presented in Table II and displayed graphically in Fig 5. The three groups were tested for measurement concordance using Friedman's analysis of variance, with a resulting *P* value of .001 and a Kendall's coefficient of concordance of 0.992, indicating excellent agreement between the three RAWD methods. Compared with the maximal manRAWD, the dirRAWD derived using manual aortic segmentation yielded a mean error of 0.25 ± 0.24 mm/y, a mean relative error of 6.5%, and no statistically significant differences between the two groups using the Wilcoxon signed rank test ($P = .69$). Comparing the manRAWD to the dirRAWD derived using semiautomated aortic segmentation yielded a mean error of 0.27 ± 0.23 mm/y, a mean relative error of 7.9%, and no statistically significant difference between the two groups using the Wilcoxon signed rank test ($P = .84$). Additionally, no difference was found between the maximal dirRAWD derived using manual AAA segmentation compared with that using semiautomated AAA segmentation by the Wilcoxon

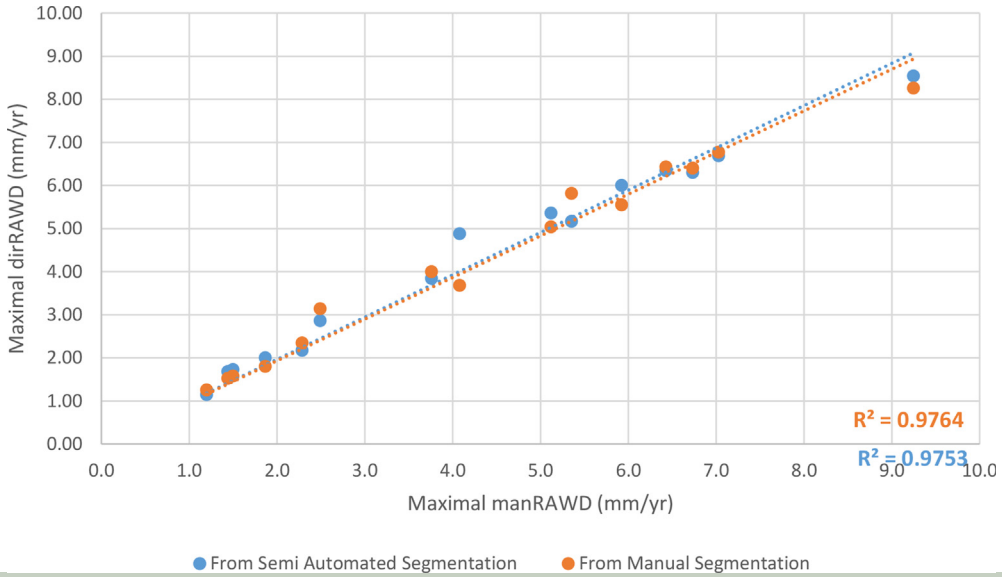

Fig 5. Scatterplot with trendline comparing true maximal aortic deformation (manRAWD) against maximal regional aortic wall deformation (RAWD) with deformable image registration (dirRAWD) for every aorta in the present study. Maximal dirRAWD derived from a manual aortic segmentation is shown in *orange*, and the maximal dirRAWD from a semiautomated aortic segmentation is displayed in *blue*.

rank sum test ($P = .55$). The intraobserver variability in calculating dirRAWD was 4.4% for manual segmentation and 5.2% for semiautomated segmentation.

Landmark displacement analysis: true vs semi-automated RAWD. The true landmark deformation, algorithm-derived landmark deformation using the manual aortic segmentation, and algorithm-derived landmark deformation using the semiautomated aortic segmentation are shown in Table III for all patients. The three groups were tested for measured landmark displacement concordance using Friedman's analysis of variance with a resulting P value of .002 and Kendall's coefficient of concordance of 0.976, indicating excellent agreement between the calculated landmark displacement values between the methods. Compared with the true landmark deformation, the algorithm-derived landmark deformation using the manual aortic segmentation resulted in a mean error of 0.67 ± 1.44 mm, a mean relative error of 13.1%, and no difference using the Wilcoxon signed rank test ($P = .39$). Compared with the true landmark deformation, the algorithm-derived landmark deformation determined using the semi-automated aortic segmentation yielded a mean error of 0.59 ± 0.93 mm, a mean relative error of 12.6%, and no difference using the Wilcoxon signed rank test ($P = .58$).

Aneurysm diameter change vs dirRAWD. The comparison of the changes in the maximal aortic diameter compared with the maximal dirRAWD is shown in Fig 6. In the eight patients with an aneurysm expansion rate <5 mm/y, excellent agreement was found between the radiographic reported maximal aortic expansion and maximal dirRAWD on linear regression ($P = .01$), with less agreement between the aortic expansion rate and maximal dirRAWD in those with expansion rates >5 mm/y ($P = .54$).

DISCUSSION

The described dirRAWD algorithm was successful in all 15 patients for whom it was attempted. These 15 patients included those with AAAs of various shapes, sizes, and amount of luminal thrombus using open source software and minimal required computational power. This technique resulted in submillimeter errors in the calculated maximal dirRAWD compared with the manRAWD (the true value), with no statistically significant differences. Furthermore, the generation of aortic segmentations was the only manual component of this pipeline, and we demonstrated no statistically significant differences in the deformable image registration error using semiautomated AAA segmentations vs manual AAA segmentations of the baseline CTA. Additionally, our methods were able to display the magnitude of local growth directly on the outer aortic wall that was more readily interpretable than prior methods, which displayed surrogated markers such as surface stress.[14]

Improvement in overall accuracy compared with maximal diameter measurements. RAWD algorithms use 3D image data along the entire length of the aorta, rather than diameters placed at fixed locations along the aortic length. The use of 3D image data results in decreased measurement error compared with measurements restricted to the axial plane, which have a reported error range of 2 to 5 mm.[5-7] Modern semiautomated rigid and deformable registration

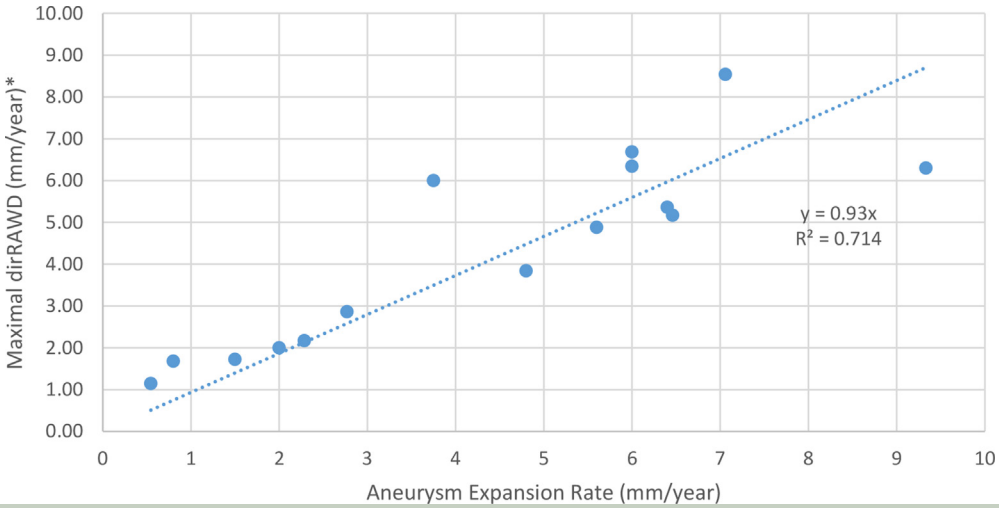

Fig 6. Scatterplot with trendline comparing radiographic reported yearly aortic expansion rate against the maximal regional aortic wall deformation (RAWD) with deformable image registration (dirRAWD) derived using the semiautomated aneurysm segmentation.

techniques, which align each location along the 3D aortic wall, have been shown to have a precision in the range of 0.5 to 1.0 mm, with our technique having a mean error of 0.24 mm (range, 0.1-0.9 mm).[15,25,26]

Superiority with 3D measurement. This technique is able to quantify a continuous range of aortic RAWD in three dimensions with associated direction and magnitude. The calculated displacement field of dirRAWD are vectors, allowing for the assessment of the direction of deformation and strain measurements, in addition to the overall magnitude. The maximal diameter techniques assume an outward radial direction to all aortic expansion in a fixed horizontal plane, which does not capture the circumferential or longitudinal components of aortic expansion. The unaccounted circumferential and longitudinal components of aortic expansion are likely to be significant in aneurysms that either have a high curvature or are a highly tortuous. The 3D nature of the dirRAWD calculations also allows for the creation of interpretable data visualization models, which are approachable for surgeons, can serve as a patient education tool, and could have utility during surgical planning.

Growth assessment away from area of maximal diameter. This algorithm models the deformation across the entire wall of the abdominal aorta and, with its increased sensitivity compared with maximal diameter methods, is able to assess for areas of small magnitude dirRAWD in regions independent of the area of the maximal diameter. This was observed in several patients in our cohort who had had subtle, but significant, aortic expansion in the proximal neck of their aorta (Fig 7). These smaller magnitude growth areas will often not be appreciated when using maximal diameter measurements but might require consideration during planning for surgical treatment of the aneurysm to avoid failure of stent-graft sealing.

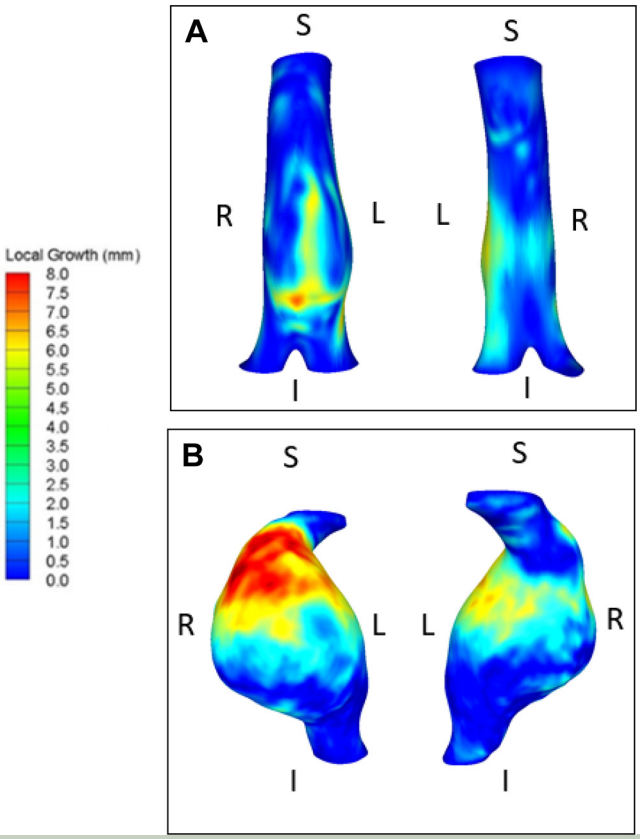

Fig 7. Two examples of regional aortic wall deformation (RAWD) with deformable image registration (dirRAWD) aortic maps generated by our process, in which maximal aortic deformation was noted to not be in the region of the maximal aneurysm diameter.

Compared with prior RAWD techniques. Our proposed dirRAWD algorithm has several advantages compared with prior reported RAWD methods. Perhaps the most significant is that our process does not use custom in-house developed scripts or software, which have been often used in prior studies.[14,25-27] The proposed method uses open-source software applications with graphic user interfaces, which are inexpensive, widely accessible, and can be implemented even by those with limited background in programming.

Previously described RAWD techniques also often required both significant user expertise in the field and dedicated high-performance computing capability, which restricted the applications to smaller centers.[14,28,29] Our deformation method can generate a RAWD heatmap on most standard powered computers for most cases within <15 minutes, with no differences in measured accuracy. Finally, prior techniques have not assessed their deformable registration models for accuracy, reporting only the accuracy seen with the rigid registration process.[14,28,29] We developed a novel approach for assessing dirRAWD accuracy in this model, comparing the maximal dirRAWD to the true aortic deformation on the rigidly registered images (man-RAWD), and assessing landmark displacement error between the second time point (ground truth) and the deformed model as a fiduciary marker.

Clinical correlation. Preliminary work by our group has shown that the aortic wall stress calculated using a finite element analysis (FEA) model might correlate and regionally colocate with RAWD and aortic expansion.[27] However, FEA accuracy is limited by the variable aneurysm wall thickness, degree of mural thrombus, and wall calcifications, which all significantly increase the model complexity and requires significant user expertise for accurate results.[30-32] Assessment of RAWD using this technique is faster than the calculation of FEA stress and is easier to interpret and understand by clinical vascular surgeons. Therefore, the technique might be a better clinical measure for guiding clinical treatment. Given the low computational power required for this novel deformation technique, it would be much easier to incorporate it into medical image viewing software compared with its FEA counterpart. As noted from our results, at increased rates of radiographic aortic expansion (>5 mm/y), we noted a significantly weaker correlation between the change in the maximal aortic diameter and aneurysm deformation. This could have resulted from aneurysms thought to have rapid radiographic diameter growth, displaying significant changes in their morphology that might not reliably be assessed with traditional maximal diameter techniques. Given that deformation calculations can better assess the entire aneurysm, this process might better guide management for this subset of patients. Additionally, because the technique uses rigid registration of the sequential CT scans, it ensures that the same area of the aneurysm will be assessed for interval changes and reduce any human measurement error. Furthermore, work is ongoing to assess the accuracy of this technique for the assessment of aneurysm shrinkage or growth after endovascular repair. This would be especially relevant for assistance in managing type II and V endoleaks. The incorporation of other previously noted geometric characteristics, in addition to the degree of deformation, would also be possible with our technique, given the aneurysm has been segmented.[9] Finally, the effects of patient clinical factors when determining the significance of aortic deformation should be assessed (ie, it is unclear whether one maximal deformation cutoff should be used for all patients or the mean deformation over an entire aneurysm wall would be more important clinically).

Technique and study limitations. The largest drawback to determining RAWD is that it requires sequential CT scans. In contrast, other methods such as FEA only require a single time-point CT. In clinical practice, this limitation will be mitigated owing to the routine AAA imaging surveillance recommended for patients with AAAs >3 cm in size and repair recommended for those with AAAs >5.5 cm.[33] The described technique, therefore, will likely be most applicable to patients requiring AAA surveillance and undergoing repeated imaging studies. Additionally, all the patients included in the present study had undergone contrast-enhanced CT scans. Work is ongoing to assess whether using non—contrast-enhanced CT scans with 2- to 3-mm slices will significantly affect final dirRAWD accuracy. This technique still requires user input for manual correction of the semiautomated aortic segmentation. However, in the present study, almost all the patients had required minimal user input (<5 minutes) for accurate dirRAWD calculations. Finally, although the present study only included 15 patients, limiting the generalizability to all patients with AAAs, we have been able to characterize this developing technique and demonstrate its accuracy.

CONCLUSIONS

The present study has demonstrated the feasibility of accurate 3D RAWD calculations with application to AAAs, which can be performed using open source software and low computing power. This process accomplishes submillimeter accuracy in determining aortic growth within a 1- to 2-year period, with minimal user input. No significant differences were found in RAWD accuracy when using manual aortic aneurysm segmentation compared with semiautomated aortic segmentation. Thus, in the future, using either semiautomated or fully automated aortic segmentation during dirRAWD calculations should be preferred because of the significant user input required for manual segmenta-

Table II. Comparison between manRAWD and algorithm-derived maximal RAWD calculated using our deformable image registration pipeline

PT. NO.	Maximal man-RAWD, mm/y	Maximal dirRAWD derived using manual segmentation, mm/y	Maximal dirRAWD derived using semiautomated segmentation, mm/y
1	1.5	1.6	1.7
2	2.5	3.1	2.9
3	1.2	1.3	1.1
4	1.4	1.5	1.7
5	5.1	5.0	5.4
6	4.1	3.7	4.9
7	2.3	2.3	2.2
8	1.9	1.8	2.0
9	5.9	5.6	6.0
10	6.4	6.4	6.3
11	6.7	6.4	6.3
12	5.4	5.8	5.2
13	3.8	4.0	3.8
14	9.2	8.3	8.5
15	7.0	6.8	6.7
MEDIAN (IQR)	4.1 (2.1-6.2)	4.0 (2.1-6.1)	4.9 (2.1-6.2)

IQR, Interquartile range; *dirRAWD,* regional aortic wall deformation using deformable image registration; *manRAWD,* manually determined maximal regional aortic wall deformation; *Pt. No.,* patient number; *RAWD,* regional aortic wall deformation.

Table III. Comparison between true IMA deformation measured manually and deformable image registration-derived IMA deformation

PT. NO.	True IMA deformation, mm/y	IMA deformation using manual segmentation, mm/y	IMA deformation using semiautomated segmentation, mm/y
1	1.2	1.1	1.0
2	1.1	1.3	1.2
3	1.0	0.9	1.1
4	1.2	1.1	1.0
5	6.5	6.4	6.5
6	3.5	3.3	3.1
7	4.2	3.7	3.8
8	2.7	2.7	2.8
9	2.0	2.1	2.1
10	8.0	5.2	5.5
11	5.0	5.0	4.6
12	7.3	7.3	6.4
13	2.5	2.6	2.5
14	6.9	12.1	10.0
15	3.8	3.3	3.4
MEDIAN (IQR)	3.5 (1.6-5.8)	3.3 (1.7 - 5.1)	3.1 (1.7 - 5.1)

IMA, Inferior mesenteric artery; *IQR,* interquartile range; *Pt. No.,* patient number.

tion. The described technique for the assessment of dirRAWD might improve the accuracy of aortic imaging surveillance, inform clinical decision-making, further research of aortic research questions, and help provide information on the natural history of aortic disease.

AUTHOR CONTRIBUTIONS

Conception and design: JS, KE, AP, AV, BJ
Analysis and interpretation: JS, KE, AP, BJ
Data collection: JS, KE
Writing the article: JS, KE, BJ
Critical revision of the article: JS, KE, AP, AV, BJ
Final approval of the article: JS, KE, AP, AV, BJ
Statistical analysis: JS
Obtained funding: Not applicable
Overall responsibility: JS

REFERENCES

1. Beckman JA. Aortic aneurysms: pathophysiology, epidemiology, and prognosis. In: Creager MA, Dzau VJ, Loscalzo J, editors. Vascular Medicine. Philadelphia, PA: Saunders Elsevier Inc; 2006.
2. Schermerhorn ML, Bensley RP, Giles KA, Hurks R, O'Malley AJ, Cotterill P, et al. Changes in abdominal aortic aneurysm rupture and short-term mortality, 1995-2008: a retrospective observational study. Ann Surg 2012;256:651-8.
3. Darling RC, Messina CR, Brewster DC, Ottinger LW. Autopsy study of unoperated abdominal aortic aneurysms: the case for early resection. Circulation 1977;56:II161-4.
4. Nicholls SC, Gardner JB, Meissner MH, Johansen KH. Rupture in small abdominal aortic aneurysms. J Vasc Surg 1998;28:884-8.
5. Hong H, Yang Y, Liu B, Cai W. Imaging of abdominal aortic aneurysm: the present and the future. Curr Vasc Pharmacol 2010;8:808-19.
6. Elefteriades JA, Farkas EA. Thoracic aortic aneurysm. J Am Coll Cardiol 2010;55:841-57.
7. Davies RR, Gallo A, Coady MA, Tellides G, Botta DM, Burke B, et al. Novel measurement of relative aortic size predicts rupture of thoracic aortic aneurysms. Ann Thorac Surg 2006;81:169-77.
8. Parr A, Jayaratne C, Buttner P, Golledge J. Comparison of volume and diameter measurement in assessing small abdominal aortic aneurysm expansion examined using computed tomographic angiography. Eur J Radiol 2011;79:42-7.
9. Pappu S, Dardik A, Tagare H, Gusberg RJ. Beyond fusiform and saccular: a novel quantitative tortuosity index may help classify aneurysm shape and predict aneurysm rupture potential. Ann Vasc Surg 2008;22:88-97.
10. Pérez EA, Rojas-Solórzano LR, Finol E. Geometric predictors of abdominal aortic aneurysm maximum wall stress. Chem Eng Trans 2016;49:73-8.
11. Georgakarakos E, Ioannou CV, Kamarianakis Y, Papaharilaou Y, Kostas T, Manousaki E, et al. The role of geometric parameters in the prediction of abdominal aortic aneurysm wall stress. Eur J Vasc Endovasc Surg 2010;39:42-8.
12. Siika A, Lindquist Liljeqvist M, Hultgren R, Gasser TC, Roy J. Aortic lumen area is increased in ruptured abdominal aortic aneurysms and correlates to biomechanical rupture risk. J Endovasc Ther 2018;25:750-6.
13. Georgakarakos E, Ioannou CV, Papaharilaou Y, Kostas T, Katsamouris AN. Computational evaluation of aortic aneurysm rupture risk: what have we learned so far? J Endovasc Ther 2011;18:214-25.
14. Burris NS, Hoff BA, Kazerooni EA, Ross BD. Vascular deformation mapping (VDM) of thoracic aortic enlargement in aneurysmal disease and dissection. Tomography 2017;3:163-73.
15. Klein S, Staring M, Pluim JPW. Evaluation of optimization methods for nonrigid medical image registration using mutual information and B-splines. IEEE Trans Image Proc 2007;16:2879-90.
16. Galbán CJ, Han MK, Boes JL, Chughtai KA, Meyer CR, Johnson TD, et al. Computed tomography-based biomarker provides unique signature for diagnosis of COPD phenotypes and disease progression. Nat Med 2012;18:1711-5.
17. Boes JL, Hoff BA, Hylton N, Pickles MD, Turnbull LW, Schott AF, et al. Image registration for quantitative parametric response mapping of cancer treatment response. Transl Oncol 2014;7:101-10.
18. Keith L, Ross BD, Galbán CJ, Luker GD, Galbán S, Zhao B, et al. Semiautomated workflow for clinically streamlined glioma parametric response mapping. Tomography 2016;2:267-75.
19. Pouch AM, Tian S, Takebe M, Yuan J, Gorman R, Cheung AT, et al. Medially constrained deformable modeling for segmentation of branching medial structures: application to aortic valve segmentation and morphometry. Med Image Anal 2015;26:217-31.
20. Yushkevich PA, Piven J, Hazlett HC, Smith RG, Ho S, Gee JC, et al. User-guided 3D active contour segmentation of anatomical structures: significantly improved efficiency and reliability. Neuroimage 2006;31:1116-28.
21. Yushkevich PA, Pluta J, Wang H, Wisse LEM, Das S, Wolk D. IC-P-174: fast automatic segmentation of hippocampal subfields and medial temporal lobe subregions in 3 Tesla and 7 Tesla T2-weighted MRI. Alzheimers Demen 2016;12:P126-7.
22. Avants BB, Epstein CL, Grossman M, Gee JC. Symmetric diffeomorphic image registration with cross-correlation: evaluating automated labeling of elderly and neurodegenerative brain. Med Image Analysis 2008;12:26-41.
23. Avants BB, Tustison NJ, Song G, Cook PA, Klein A, Gee JC. A reproducible evaluation of ANTs similarity metric performance in brain image registration. Neuroimage 2011;54:2033-44.
24. Zijdenbos AP, Dawant BM, Margolin RA, Palmer AC. Morphometric analysis of white matter lesions in MR images: method and validation. IEEE Trans Med Imaging 1994;13:716-24.
25. Gao X, Boccalini S, Kitslaar PH, Budde RP, Tu S, Lelieveldt BP, et al. A novel software tool for semi-automatic quantification of thoracic aorta dilatation on baseline and follow-up computed tomography angiography. Int J Cardiovasc Imaging 2019;35:711-23.
26. Kauffmann C, Tang A, Therasse E, Giroux M-F, Elkouri S, Melanson P, et al. Measurements and detection of abdominal aortic aneurysm growth: accuracy and reproducibility of a segmentation software. Eur J Radiol 2012;81:1688-94.
27. Auer M, Gasser TC. Reconstruction and finite element mesh generation of abdominal aortic aneurysms from computerized tomography angiography data with minimal user interactions. IEEE Trans Med Imaging 2010;29:1022-8.
28. López-Linares K, García I, García A, Cortes C, Piella G, Macía I, et al. Image-based 3D characterization of abdominal aortic aneurysm deformation after endovascular aneurysm repair. Front Bioeng Biotechnol 2019;7:267.
29. Subasic M, Loncaric S, Sorantin E. 3-D image analysis of abdominal aortic aneurysm. Stud Health Technol Inform 2000;77:1195-200.
30. Shang EK, Nathan DP, Sprinkle SR, Vigmostad SC, Fairman RM, Bavaria JE, et al. Peak wall stress predicts expansion rate in descending thoracic aortic aneurysms. Ann Thorac Surg 2013;95:593-8.
31. Gasser TC, Auer M, Labruto F, Swedenborg J, Roy J. Biomechanical rupture risk assessment of abdominal aortic aneurysms: model complexity versus predictability of finite element simulations. Eur J Vasc Endovasc Surg 2010;40:176-85.
32. Polzer S, Gasser TC, Bursa J, Staffa R, Vlachovsky R, Man V, et al. Importance of material model in wall stress prediction in abdominal aortic aneurysms. Med Eng Phys 2013;35:1282-9.
33. Chaikof EL, Dalman RL, Eskandari MK, Jackson BM, Lee WA, Mansour MA, et al. The Society for Vascular Surgery practice guidelines on the care of patients with an abdominal aortic aneurysm. J Vasc Surg 2018;67:2-77.e2.

Submitted Mar 31, 2021; accepted Nov 17, 2021.

Supplementary Table. Detailed demographics of 15 included patients

Pt. No.	Age, years	Sex	Hypertension	Statin use	eGFR, mL/min	Family history of aneurysm	True maximal deformation, mm/y	Initial maximal aortic diameter, mm	Final maximal aortic diameter, mm
1	63	M	Yes	No	90	No	1.5	42	44
2	79	M	No	Yes	50	No	2.5	39	42
3	73	M	Yes	Yes	70	No	1.2	31	32
4	83	F	Unknown	Unknown	70	No	1.4	31	32
5	72	M	Yes	Yes	80	Yes	5.1	45	53
6	70	F	No	No	70	No	4.1	55	62
7	62	F	Yes	Yes	90	No	2.3	27	31
8	59	M	Yes	No	110	No	1.9	51	54
9	46	M	Yes	No	120	Yes	5.9	60	65
10	58	F	Yes	Yes	100	No	6.4	36	43
11	46	M	Yes	No	120	No	6.7	44	58
12	68	F	No	No	90	No	5.4	48	55
13	80	F	No	Yes	50	No	3.8	32	38
14	77	M	Yes	Yes	80	No	9.2	54	64
15	65	M	Yes	No	90	Yes	7.0	45	52

eGFR, Estimated glomerular filtration rate (using the Chronic Kidney Disease Epidemiology Collaboration creatinine equation, 2021); *F,* female; *M,* male.

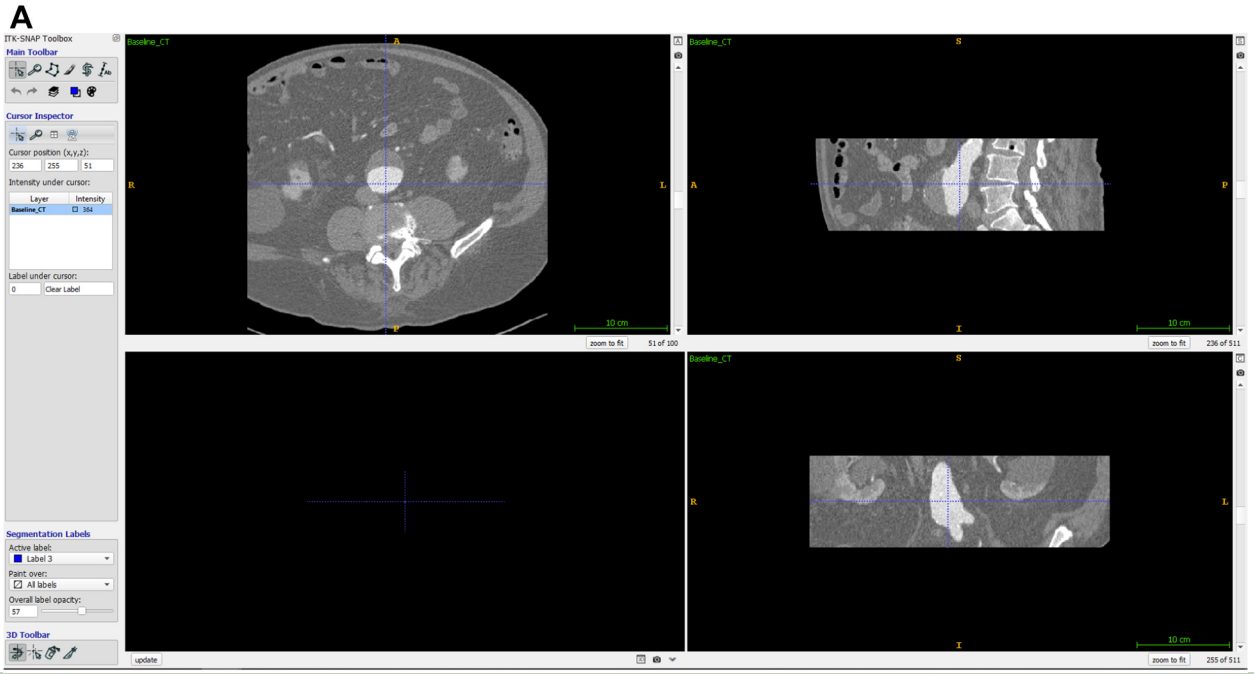

Supplementary Fig. A, Baseline computed tomography angiogram (CTA) as shown in ITK-SNAP. **B,** Baseline CTA with single label segmentation of the aortic aneurysm. ITK-SNAP is able to automatically generate a 3D model of the segmentation (lower left) and export this as a mesh of the outer wall of the aortic aneurysm. **C**, Baseline CTA and aneurysm segmentation compared with follow-up CTA as shown in ITK-SNAP. Initially, a significant translational difference was present between the two CTAs, as noted in the sagittal and coronal images, which had led to initial poor alignment of the aneurysm between scans. **D**, Baseline CTA and dilated aortic aneurysm segmentation compared with follow-up CTA, as shown in ITK-SNAP. Dilated segmentation was used during both rigid and deformable registration to restrict the algorithms to the area of interest and improve both accuracy and efficiency. **E,** Baseline CTA and dilated aneurysm segmentation compared with follow-up CTA, as shown in ITK-SNAP after rigid registration. Initial rigid registration was performed using a multiresolution scheme with 16× to 8× down-sampling to grossly align the images. Rigid registration was then repeated with computation of the similarity metric confined to the dilated aortic segmentation, first with 4× down-sampling and then at full resolution. **F,** Baseline CTA and aneurysm segmentation compared with follow-up CTA, as shown in ITK-SNAP, after rigid registration. Excellent alignment can now be visualized between the two time points in both the aneurysm and bony landmarks. The difference between the size of the baseline aneurysm segmentation and the follow-up CTA aneurysm size indicated interval growth of the aneurysm. The rigid registration matrix (detailing the amount of translation required to align the images) was then exported to a text file. *Greedy* was then used with the baseline CTA, follow-up CTA, dilated aneurysm segmentation, and rigid registration matrix to automatically generate a 3D deformation field. For deformable image registration, we used a normalized cross-correlation similarity metric with a gradient descent optimization for 100 iterations at a course level of 4×, 50 iterations at an intermediate level of 2×, and 20 iterations at full resolution. For further algorithm optimization, the deformable registration was limited to a 10 × 10 × 10 neighborhood around each voxel, and the baseline aortic segmentation was dilated by 1.5 cm and used to restrict the deformation algorithm to the area of interest. A smoothing gradient with a sigma of 1.732 voxels was applied to the image match metric at each voxel, and the entire deformation field was smoothed with a gradient sigma of 0.707 voxel after each iteration to limit error and generate a smooth field. **G,** Baseline aneurysm segmentation on the left compared with the 3D deformation field on the right (displayed as the magnitude of deformation, with *white* indicating increased deformation). **F,** As expected from the rigid registration results, maximal deformation was noted at the anterior wall of the aneurysm. **H,** The patient's baseline aneurysm mesh is displayed (**Left**) as shown in MeshLab. (**Center**) *Greedy* was used to apply the 3D deformation field to this baseline aneurysm mesh. (**Right**) Magnitude difference experienced by every vertex on the baseline aneurysm mesh with application of the deformation field (ie, difference between the left and middle images) with smoothing to remove segmentation artifact.

B

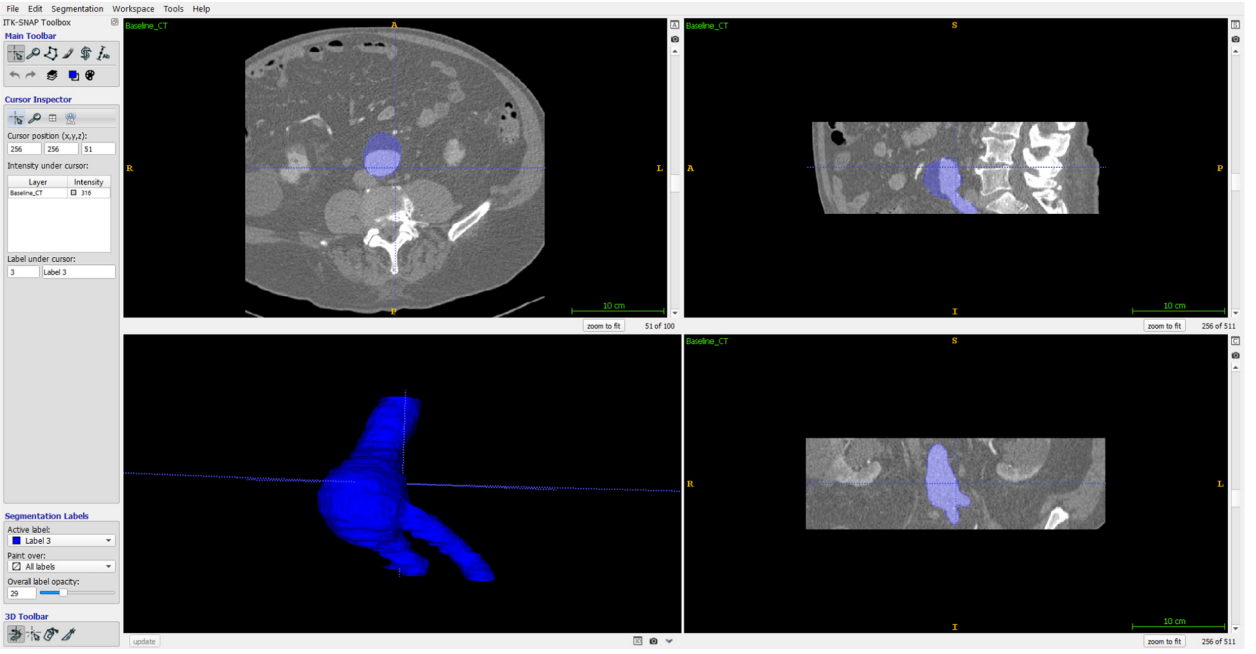

C

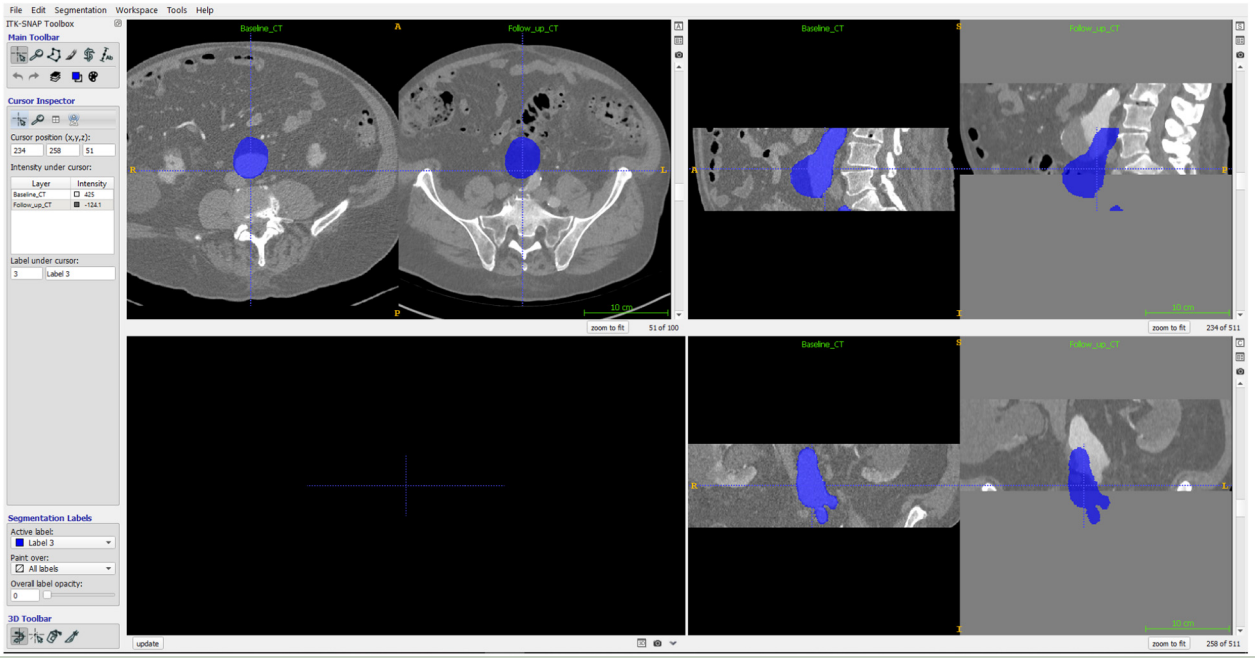

Supplementary Fig. (Continued).

D

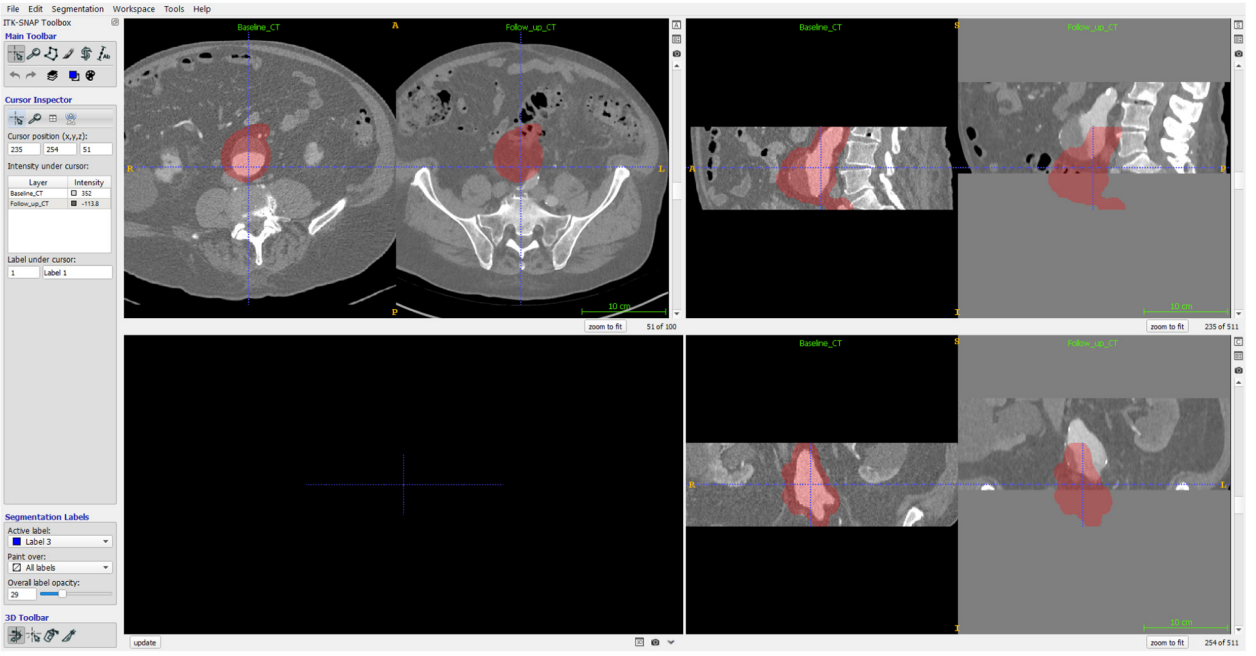

E

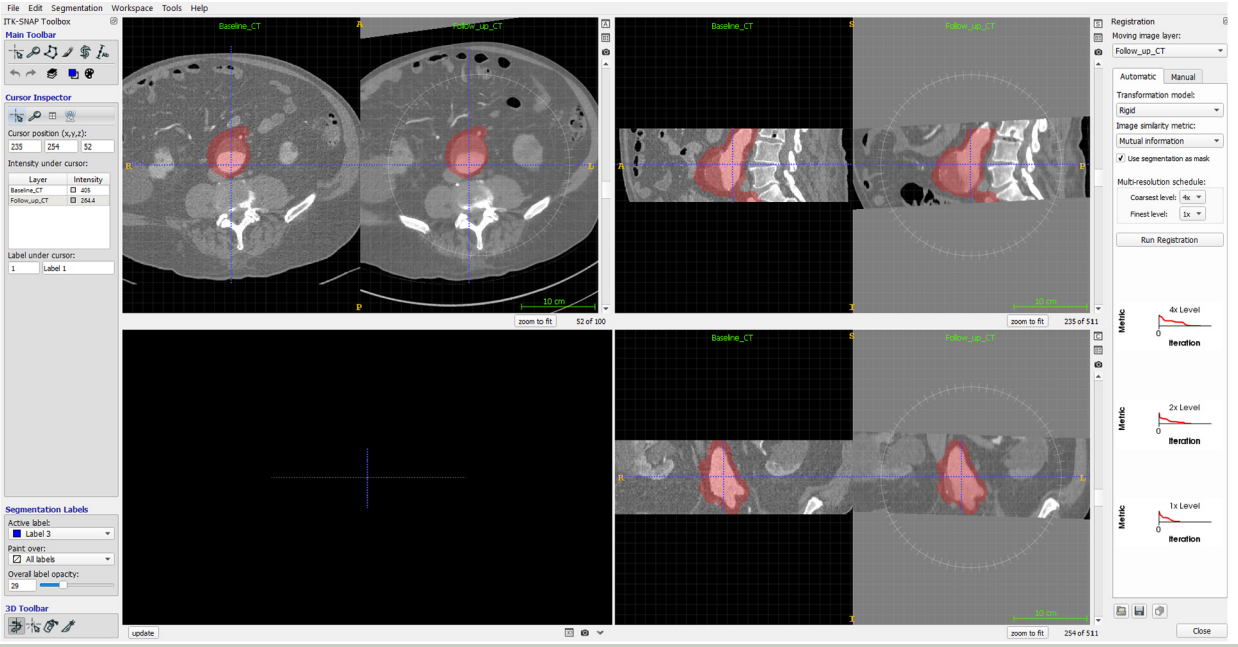

Supplementary Fig. (Continued).

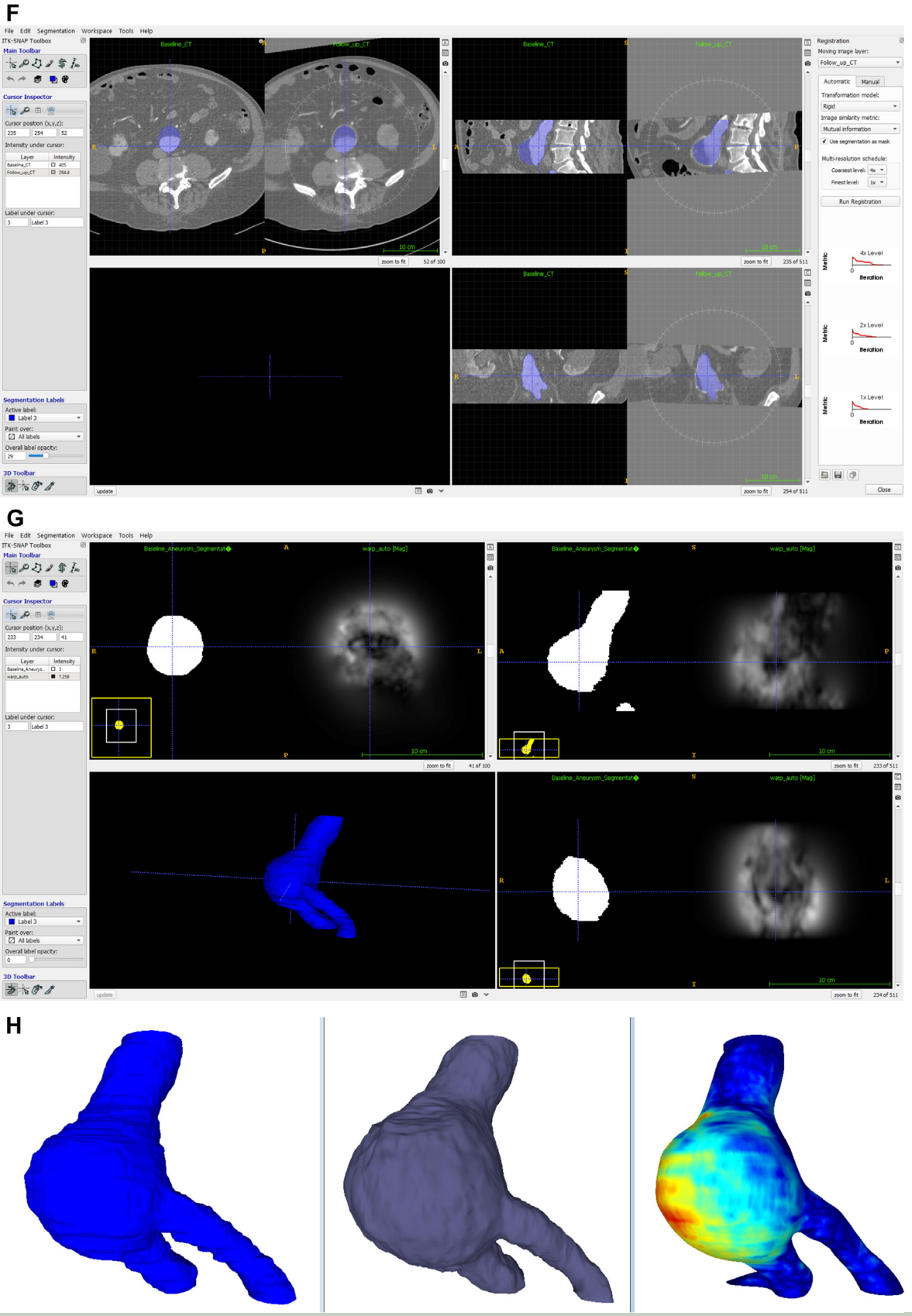

Supplementary Fig. (Continued).